

Exploring the complex X-ray spectrum of NGC 4051.

K.A.Pounds¹, J.N.Reeves², A.R.King¹ and K.L.Page,¹

¹ Department of Physics and Astronomy, University of Leicester, Leicester, LE1 7RH, UK

² Laboratory for High Energy Astrophysics, NASA Goddard Space Flight Center, Greenbelt, MD 20771, USA

Accepted ; Submitted

ABSTRACT

Archival *XMM-Newton* data on the nearby Seyfert galaxy NGC 4051, taken in relatively high and low flux states, offer a unique opportunity to explore the complexity of its X-ray spectrum. We find the hard X-ray band to be significantly affected by reflection from cold matter, which can also explain a non-varying, narrow Fe K fluorescent line. We interpret major differences between the high and low flux hard X-ray spectra in terms of the varying ionisation (opacity) of a substantial column of outflowing gas. An emission line spectrum in the low flux state indicates an extended region of photoionised gas. A high velocity, highly ionised outflow seen in the high state spectrum can replenish the gas in the extended emission region over $\sim 10^3$ years, while having sufficient kinetic energy to contribute significantly to the hard X-ray continuum.

Key words: galaxies: active – galaxies: Seyfert: general – galaxies: individual: NGC 4051 – X-ray: galaxies

1 INTRODUCTION

The additional sensitivity of *XMM-Newton* and *Chandra* has emphasised the complexity in the X-ray spectra of AGN. While there is broad agreement that the X-ray emission is driven by accretion onto a supermassive black hole, the detailed emission mechanism(s) remain unclear. Significant complexity - and diagnostic potential - is introduced by reprocessing of the primary X-rays in surrounding matter. Scattering and fluorescence from dense matter in the putative accretion disc has been recognised as a major factor in modifying the observed X-ray emission of bright Seyfert galaxies since its discovery 13 years ago (Nandra et al. 1989, Pounds et al. 1990). Additional modification of the observed X-ray spectra arises by absorption in passage through ionised matter in the line of sight to the continuum X-ray source. The high resolution X-ray spectra obtained with *XMM-Newton* and *Chandra* have shown the considerable complexity of this ‘warm absorber’ (eg Sako et al. 2001, Kaspi et al. 2002), including recent evidence for high velocity outflows (eg Chartas et al. 2002, Pounds et al. 2003a,b; Reeves et al. 2003) which constitute a significant component in the mass and energy budgets of those AGN. In this paper we report on the spectral analysis of two *XMM-Newton* observations of the bright, nearby Seyfert 1 galaxy NGC 4051 taken from the *XMM-Newton* data archive. We find further support for the suggestion made in an early survey of *XMM-Newton* Seyfert spectra (Pounds and Reeves 2002), that the full effects of ionised absorption in AGN have often been underestimated.

NGC 4051 is a low redshift ($z = 0.0023$) narrow line Seyfert 1 galaxy, which has been studied over much of the history of X-ray astronomy. Its X-ray emission often varies rapidly and with a large amplitude (Lawrence et al. 1985, 1987), occasionally lapsing into extended periods of extreme low activity (Lamer et al. 2003). When bright, the broad band X-ray spectrum of NGC 4051 appears typical of a Seyfert 1 galaxy, with a 2–10 keV continuum being well represented by a power law of photon index $\Gamma \sim 1.8$ –2, with a hardening of the spectrum above ~ 7 keV being attributable to ‘reflection’ from ‘cold’, dense matter, which might also be the origin of a relatively weak Fe K emission line (Nandra and Pounds 1994). However, NGC 4051 also exhibits strong spectral variability, apparently correlated with source flux. The nature of this spectral variability has remained controversial since the *GINGA* data were alternatively interpreted as a change in power law slope (Matsuoka et al. 1990) and by varying partial covering of the continuum source by optically thick matter (Kunieda et al. 1992).

Later *ROSAT* observations provided good evidence for a flux-linked variable ionised absorber, and for a ‘soft excess’ below ~ 1 keV (Pounds et al. 1994, McHardy et al. 1995, Komossa and Fink 1997). Extended *ASCA* observations led Guainazzi et al. (1996) to report a strong and broad Fe K emission line (implying reflection from the inner accretion disc), and a positive correlation of the hard power law slope with X-ray flux. A 3-year monitoring campaign of NGC 4051 with *RXTE*, including a 150-day extended low interval in 1998, produced clear evidence for the cold reflection component (hard continuum and narrow 6.4 keV Fe K line) re-

maining constant, while again finding the residual power law slope to steepen at higher X-ray fluxes (Lamer et al. 2003). More surprisingly, a relativistic broad Fe K line component was found to be always present, even during the period when the Seyfert nucleus was ‘switched off’ (Guainazzi et al. 1998, Lamer et al. 2003). One other important contribution to the extensive X-ray literature on NGC 4051 came from an early *Chandra* observation which resolved two X-ray absorption line systems, with outflowing velocities of ~ 2300 and ~ 600 km s^{-1} , superimposed on a continuum soft excess with significant curvature (Collinge et al. 2001). Of particular interest in the context of the present analysis, the higher velocity outflow is seen in lines of the highest ionisation potential. The *Chandra* data also show an unresolved Fe K emission line at ~ 6.41 keV (FWHM ≤ 2800 km s^{-1}).

In summary, no clear picture emerges from a review of the extensive data on the X-ray spectrum of NGC 4051, with the spectral variability being (mainly) due to a strong power law slope - flux correlation, or to variable absorption in (a substantial column of) ionised matter. Support for the former view has recently come from a careful study of the soft-to-hard flux ratios in extended *RXTE* data (Taylor et al. 2003), while the potential importance of absorption is underlined by previous spectral fits to NGC 4051 requiring column densities of order $\sim 10^{23}$ cm^{-2} (eg Pounds et al. 1994, McHardy et al. 1995).

Given these uncertainties we decided to extract *XMM-Newton* archival data on NGC 4051 in order to explore its spectral complexities. After submission of the present paper, an independent analysis of the 2002 November EPIC pn data by Uttley et al. (2003) was published on astro-ph, reaching different conclusions to those we find. We comment briefly on these alternative descriptions of the spectral variability of NGC 4051 in Section 9.4.

2 OBSERVATION AND DATA REDUCTION

NGC 4051 was observed by *XMM-Newton* on 2001 May 16/17 (orbit 263) for ~ 117 ksec, and again on 2002 November 22 (orbit 541) for ~ 52 ksec. The latter observation was timed to coincide with an extended period of low X-ray emission from NGC 4051. These data are now public and have been obtained from the *XMM-Newton* data archive. X-ray data are available in both observations from the EPIC pn (Strüder et al. 2001) and MOS2 (Turner et al. 2001) cameras, and the Reflection Grating Spectrometer/RGS (den Herder et al. 2001). The MOS1 camera was also in spectral mode in the 2002 observation. Both EPIC cameras were used in small window mode in the first observation, together with the medium filter, successfully ensuring negligible pile-up. The large window mode, with medium filter, was used in the second, low flux state observation. The X-ray data were first screened with the latest XMM SAS v5.4 software and events corresponding to patterns 0-4 (single and double pixel events) were selected for the pn data and patterns 0-12 for MOS1 and MOS2. A low energy cut of 300 eV was applied to all X-ray data and known hot or bad pixels were removed. We extracted EPIC source counts within a circular region of $45''$ radius defined around the centroid position of NGC 4051, with the background being taken from a similar region, offset from but close to the source. The net exposures

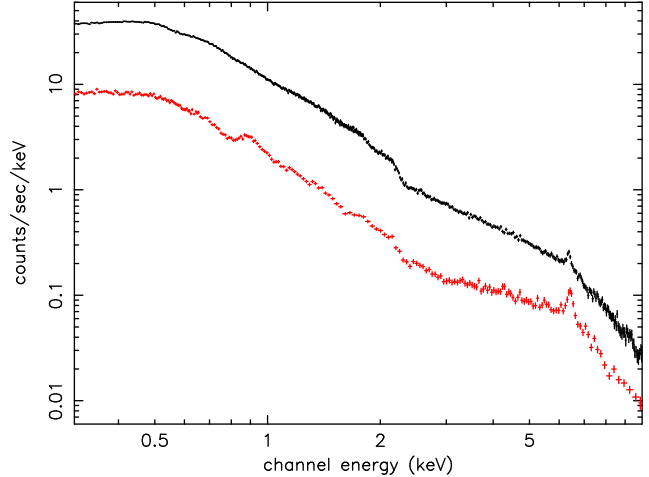


Figure 1. Background-subtracted EPIC pn data for the 2001 May (black) and 2002 November (red) observations of NGC 4051

available for spectral fitting from the 2001 observation were 81.7 ksec (pn), 103.6 ksec (MOS2), 114.3 ksec (RGS1) and 110.9 ksec (RGS2). For the 2002 observation the final spectral data were of 46.6 ksec (pn), 101.9 ksec (MOS1 and 2), 51.6 ksec (RGS1) and 51.6 ksec (RGS2). Data were then binned to a minimum of 20 counts per bin, to facilitate use of the χ^2 minimisation technique in spectral fitting. Spectral fitting was based on the Xspec package (Arnaud 1996). All spectral fits include absorption due to the NGC 4051 line-of-sight Galactic column of $N_H = 1.32 \times 10^{20} \text{ cm}^{-2}$ (Elvis et al. 1989). Errors are quoted at the 90% confidence level ($\Delta\chi^2 = 2.7$ for one interesting parameter).

We analysed the broad-band X-ray spectrum of NGC 4051 integrated over the separate *XMM-Newton* observations, noting the mean flux levels were markedly different, and perhaps representative of the ‘high state’ and ‘low state’ X-ray spectra of this Seyfert galaxy. [In fact the 2001 May X-ray flux is close to the historical mean for NGC 4051, but we will continue to refer to it as the ‘high state’ for convenience]. To obtain a first impression of the spectral change we compare in figure 1 the background-subtracted spectra from the EPIC pn camera for orbits 263 and 541. The same comparison for the EPIC MOS2 data (not shown) is essentially identical. From ~ 0.3 – 3 keV the spectral shape is broadly unchanged, with the 2001 flux level being a factor ~ 5 higher. From ~ 3 keV up to the very obvious emission line at ~ 6.4 keV the flux ratio decreases, indicating a flatter continuum slope in the low state spectrum over this energy band. On this simple comparison the ~ 6.4 keV emission line appears essentially unchanged in energy, width and photon flux. We will defer a more detailed comparison of the ‘high’ and ‘low’ state data until Section 5, after first modelling the individual EPIC spectra.

3 HIGH STATE EPIC SPECTRUM

3.1 Power law continuum

We began our analysis of the EPIC data for 2001 May in the conventional way by fitting a power law over the hard X-ray (3–10 keV) band, thereby excluding the more obvious effects

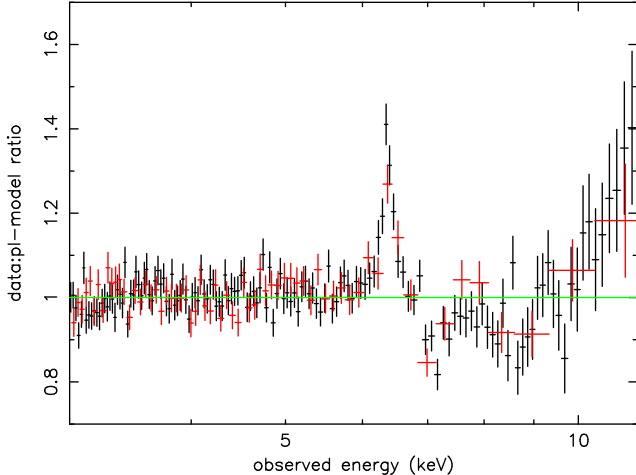


Figure 2. Ratio of data to power law fits over the 3–10 keV band for the pn (black) and MOS (red) spectra in the high state 2001 May observation of NGC 4051.

of soft X-ray emission and/or low energy absorption. This fit yielded a photon index of $\Gamma \sim 1.85$ (pn) and $\Gamma \sim 1.78$ (MOS), but the fit was poor with significant residuals. In particular the presence of a narrow emission line near 6.4 keV, and increasing positive residuals above 9 keV (figure 2), suggested the addition of a cold reflection component to refine the continuum fit, which we then modelled with PEXRAV in Xspec (Magdziarz and Zdziarski 1995). Since the reflection component was not well constrained by the continuum fit, we left free only the reflection factor R ($= \Omega/2\pi$, where Ω is the solid angle subtended at the source), fixing the power law cut-off at 200 keV and disc inclination at 20° , with all abundances solar. The outcome was an improved fit, with $\Delta\chi^2$ of 40 for $R = 0.8 \pm 0.2$. The power law index Γ increased by 0.1 for both pn and MOS fits. In all subsequent fits we then set $R = 0.8$ (compatible with the strength of the 6.4 keV emission line). Based on this broad band fit we obtained a 2–10 keV flux for the 2001 May observation of NGC 4051 of 2.4×10^{-11} erg s $^{-1}$ cm $^{-2}$ corresponding to a 2–10 keV luminosity of 2.7×10^{41} erg s $^{-1}$ ($H_0 = 75$ km s $^{-1}$ Mpc $^{-1}$).

3.2 Fe K emission and absorption

The power law plus reflection continuum fit at 3–10 keV leaves several residual features in both pn and MOS data, the significance of which are indicated by the combined χ^2 of 2068 for 1740 degrees of freedom (dof). Visual examination of figure 2 shows, in particular, a narrow emission line near 6.4 keV and evidence of absorption near ~ 7 keV and between ~ 8 –9 keV.

To quantify these features we then added further spectral components to the model, beginning with a gaussian emission line with energy, width and equivalent width as free parameters. This addition improved the 3–10 keV fit, to χ^2/dof of 1860/1735, with a line energy (in the AGN rest frame) of 6.38 ± 0.01 keV (pn) and 6.42 ± 0.03 keV (MOS), rms width ≤ 60 eV and line flux of $1.6 \pm 0.4 \times 10^{-5}$ photon s $^{-1}$ cm $^{-2}$ (pn) and $1.4 \pm 0.6 \times 10^{-5}$ photon s $^{-1}$ cm $^{-2}$ (MOS), corresponding to an equivalent width (EW) of 60 ± 15 eV.

Next, we fitted the most obvious absorption feature near 7 keV with a gaussian shaped absorption line, again with

energy, width and equivalent width free. The best-fit observed line energy was 7.15 ± 0.05 keV (pn) and 7.05 ± 0.05 keV (MOS) in the AGN rest-frame, with an rms width of 150 ± 50 eV, and an EW of 100 ± 20 eV. The addition of this gaussian absorption line gave a further highly significant improvement to the overall fit, with $\chi^2/\text{dof} = 1802/1730$. Fitting the less compelling absorption feature at ~ 8 –9 keV with a second absorption line was not statistically significant. However, an absorption edge did improve the fit to $\chi^2/\text{dof} = 1767/1728$, for an edge energy of 8.0 ± 0.1 keV and optical depth 0.15 ± 0.05 .

In summary, the 3–10 keV EPIC data from the high state 2001 May observation of NGC 4051 is dominated by a power law continuum, with a photon index (after inclusion of cold reflection plus an emission and absorption line) of 1.90 ± 0.02 (pn) and 1.84 ± 0.02 (MOS). The narrow emission line at ~ 6.4 keV is compatible with fluorescence from the same cold reflecting matter, while - if identified with resonance absorption of FeXXVI or FeXXV - the ~ 7.1 keV line implies a substantial outflow of highly ionised gas. We find no requirement for the previously reported strong, broad Fe K emission line, the formal upper limit for a line of initial energy 6.4 keV being 70 eV.

3.3 Soft Excess

Extending the above 3–10 keV continuum spectral fit down to 0.3 keV, for both pn and MOS data, shows very clearly (figure 3) the strong soft excess indicated in earlier observations of NGC 4051.

To quantify the soft excess we again fitted the combined pn and MOS data, obtaining a reasonable overall fit with the addition of blackbody continua of $kT \sim 120$ and 270 eV, together with absorption edges at ~ 0.725 keV ($\tau \sim 0.24$) and ~ 0.88 keV ($\tau \sim 0.09$). Based on this broad band fit we deduced soft X-ray flux levels for the 2001 May observation of NGC 4051 of 2.9×10^{-11} erg s $^{-1}$ cm $^{-2}$ (0.3–1 keV), with ~ 61 percent in the blackbody components, and 1.1×10^{-11} erg s $^{-1}$ cm $^{-2}$ (1–2 keV). Combining these results with the higher energy fit yields an overall 0.3–10 keV luminosity of NGC 4051 in the ‘high’ state of 7×10^{41} erg s $^{-1}$ ($H_0 = 75$ km s $^{-1}$ Mpc $^{-1}$).

4 LOW STATE EPIC SPECTRUM

The above procedure was then repeated in an assessment of the 2002 November EPIC data, when the X-ray flux from NGC 4051 was a factor ~ 4.5 lower (figure 1).

Fitting the hard X-ray continuum was now more uncertain since the spectrum was more highly curved in the low flux state (compare figs 4 and 2), making an underlying power law component difficult to identify. To constrain the fitting parameters we therefore made two important initial assumptions. The first, supported by the minimal change apparent in the narrow Fe K line, was to carry forward the cold reflection (normalisation and R) parameters from the ‘high state’ spectral fit (in fact, as noted above, appropriately at a flux level close to the historical average for NGC 4051). The second assumption was that the power law continuum changed only in normalisation, but not in slope (as

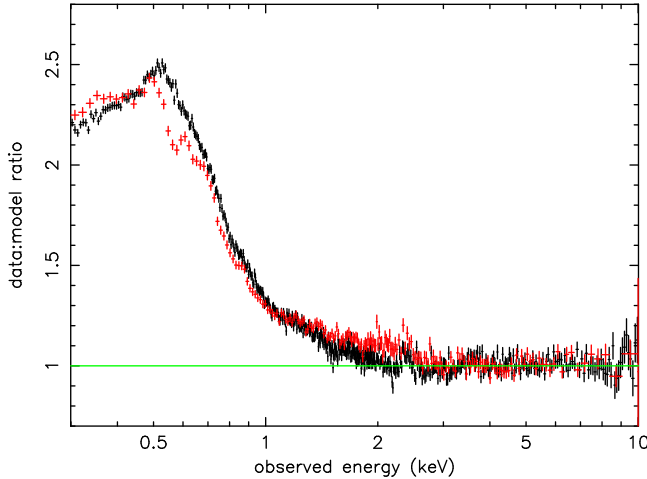


Figure 3. Extrapolation to 0.3 keV of the 3–10 keV spectral fit (detailed in section 3.2) showing the strong soft excess in both pn (black) and MOS (red) spectra during the 2001 May observation of NGC 4051.

found in the extended *XMM-Newton* observation of MCG-6-30-15, Fabian and Vaughan 2003). This is in contrast to the conclusions of Lamer et al. (2003) but - as we see later - is consistent with the difference spectrum (figure 8), which fits quite well at 3–10 keV to a power law slope of $\Gamma \sim 2$, while also showing no significant residual reflection features.

With these initial assumptions, the 3–10 keV fit to the low state spectrum yielded the data:model ratio shown in figure 4. A visual comparison with figure 2 shows a very similar narrow emission line at ~ 6.4 keV, but with strong curvature to the underlying continuum, and significant differences in the absorption features above 7 keV. These strong residuals resulted in a very poor fit at 3–10 keV, with χ^2 of 1610/990. We note the spectral curvature in the 3–6 keV band is reminiscent of an extreme relativistic Fe K emission line; however, since our high state spectrum showed no evidence for such a feature, and it might in any case be unexpected when the hard X-ray illumination of the innermost accretion disc is presumably weak, we considered instead a model in which a fraction of the power law continuum is obscured by an ionised absorber. We initially modelled this possibility with ABSORI in Xspec, finding both the 3–6 keV spectral curvature and the absorption edge at ~ 7.6 keV were well fitted with ~ 60 percent of the power law covered by ionised matter of ionisation parameter $\xi (=L/nr^2) \sim 25$ and column density $N_H \sim 1.2 \times 10^{23} \text{ cm}^{-2}$.

The main residual feature was then the narrow Fe K emission line.

4.1 The narrow Fe K emission line

A gaussian line fit to the emission line at ~ 6.4 keV in the low state EPIC data was again unresolved, with a mean energy (in the AGN rest frame) of 6.41 ± 0.01 keV (pn) and 6.39 ± 0.02 keV (MOS), and line fluxes of $1.9 \pm 0.3 \times 10^{-5}$ photon $\text{s}^{-1} \text{cm}^{-2}$ (pn) and $2.0 \pm 0.4 \times 10^{-5}$ photon $\text{s}^{-1} \text{cm}^{-2}$ (MOS), corresponding to an EW against the unabsorbed power law component of 500 ± 75 eV. The important point is that, within the measurement errors, the measured fluxes of the ~ 6.4 keV line are the same for the two observations.

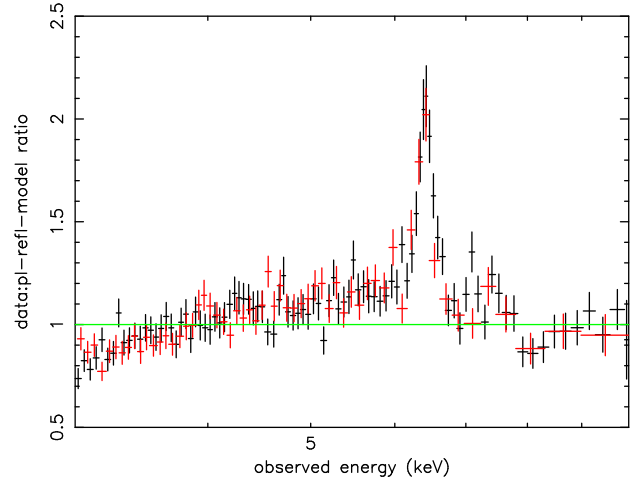


Figure 4. Ratio of data to power law plus continuum reflection model fit over the 3–10 keV band for the pn (black) and MOS (red) spectra in the low state 2002 November observation of NGC 4051.

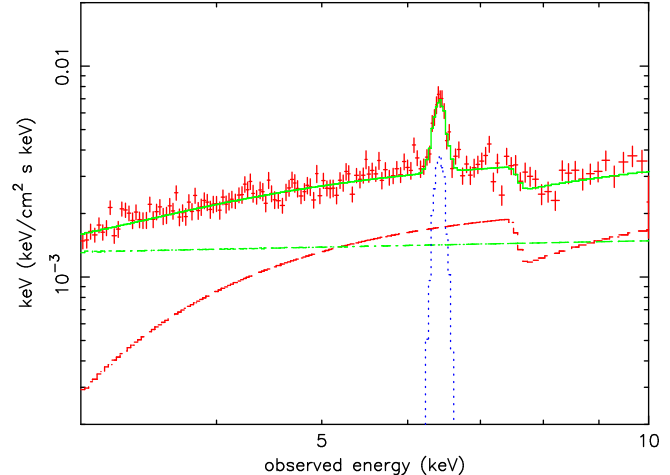


Figure 5. Partial covering model spectrum fitted over the 3–10 keV band for the 2002 November observation of NGC 4051. Also shown are the separate components in the fit: the unabsorbed power law (green), absorbed power law (red) and Gaussian emission line (blue). See Section 4.1 for details. For clarity only the pn data are shown.

This lends support to our initial assumption that both EPIC spectra include a ‘constant’ reflection component, illuminated by the long-term average hard X-ray emission from NGC 4051. With the addition of this narrow emission line the overall 3–10 keV fit obtained with the partial covering model was then good ($\chi^2/\text{dof} = 1037/1037$). Figure 5 illustrates the unfolded spectrum and spectral components of this fit.

4.2 Soft Excess

Extrapolation of the above partial covering 3–10 keV spectral fit down to 0.3 keV shows a substantial soft X-ray excess remains (figure 6), with a similar relative strength to the power law component seen in the high state data. We note that the ‘soft excess’, ie relative to the power law component,

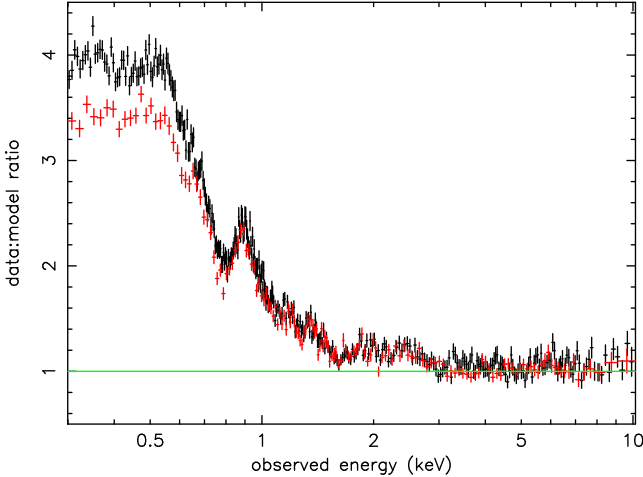


Figure 6. Partial covering model fits over the 3–10 keV band extended to 0.3 keV, for the pn (black) and MOS (red) data from the low state 2002 November observation of NGC 4051.

would have been extremely strong (data: model ratio ~ 8) had we taken the simple power law fit ($\Gamma\sim 1.4$) to the low state 3–10 keV data. Extending the partial covering model to 0.3 keV, with the addition - as in the high state - of a blackbody component of $kT\sim 125$ eV (the hotter component was not required), gave an initially poor fit (χ^2 of 2348 for 1265 dof for the pn data), with a broad deficit in observed flux at ~ 0.7 – 0.8 keV being a major contributor (figure 6). The addition of a gaussian absorption line to the partial covering model gave a large improvement to the broad-band fit (to χ^2 of 1498 for 1262 dof), for a line centred at 0.756 ± 0.003 keV, with rms width 50 ± 15 eV and EW ~ 40 eV. We show this complex spectral fit in figure 7, and comment that the model dependency of unfolded spectra is relatively unimportant in illustrating such strong, broad band spectral features. Significantly, the broad-band spectral fit remains substantially inferior to the similar fit to the high state data. Examination of the spectral residuals shows this is due to additional fine structure in the soft band of the low state spectrum, structure that is also evident in figures 6 and 7. We examine the RGS data in Section 6 to explore the nature (absorption or emission) of this structure.

The deduced soft X-ray flux levels for the 2002 November observation of NGC 4051 were 6.3×10^{-12} erg s $^{-1}$ cm $^{-2}$ (0.3–1 keV), with ~ 53 percent in the blackbody component, and 1.8×10^{-12} erg s $^{-1}$ cm $^{-2}$ (1–2 keV). Combining these results with a 2–10 keV flux of 5.8×10^{-12} erg s $^{-1}$ cm $^{-2}$ yielded an overall 0.3–10 keV luminosity of NGC 4051 in the ‘low’ state of 1.5×10^{41} erg s $^{-1}$ ($H_0=75$ km s $^{-1}$ Mpc $^{-1}$).

5 COMPARISON OF THE HIGH AND LOW STATE EPIC DATA

The above spectral fitting included two important assumptions, that the cold reflection was unchanged between the high and low flux states, and the variable power law component was of constant spectral index. We now compare the EPIC data for the two observations to further explore the nature of the spectral change. Figure 8 illustrates the difference spectrum obtained by subtracting the background-

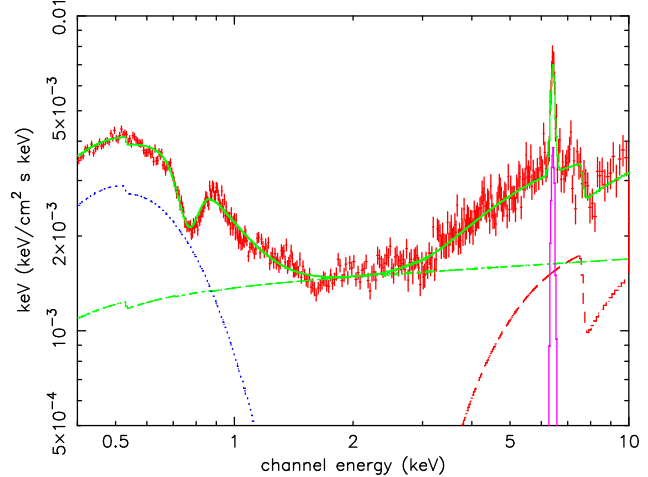


Figure 7. Extrapolation to 0.3 keV of the 3–10 keV partial covering fit of fig 5 showing the strong soft excess modelled by a blackbody component (blue), and a broad absorption trough at ~ 0.76 keV. For clarity only the pn data are shown.

subtracted low state data from the equivalent high state data (corrected for exposure). To improve the statistical significance of the higher energy points the data were re-grouped for a minimum of 200 counts. The resulting difference spectrum is compared in figure 8 with a power law fitted at 3–10 keV. Several points are of interest. First, the power law index of the difference spectrum, $\Gamma\sim 2.04$ (pn) and $\Gamma\sim 1.97$ (M2), is consistent with the assumed ‘constant’ value in the individual spectral fits. Second, the narrow Fe K emission line and high energy data upturn are not seen, supporting our initial assumption of a ‘constant’ cold reflection component. The narrow feature observed at ~ 7 keV corresponds to the absorption line seen (only) in the high state spectrum, while we shall see in Section 6 that the deficit near 0.55 keV in the MOS data (which has substantially better energy resolution there than the pn) is probably explained by a strong and ‘constant flux’ emission line of OVII. Finally, the small peak near 8 keV can be attributed to the absorption edge shifting to lower energy as the photoionised gas recombines in the reduced continuum irradiation.

While the arithmetic difference of two spectra provides a sensitive check for the variability of additive spectral components, a test of the variability of multiplicative components is provided by the ratio of the respective data sets. Figure 9 reproduces the ratio of the high and low state data (pn only) after re-grouping to a minimum of 500 counts per bin. From ~ 0.3 – 3 keV the flux ratio averages ~ 5 , as seen in figure 1, falling to higher energies as the mean slope of the low state spectrum hardens. The large positive feature at ~ 0.7 – 0.8 keV is of particular interest, indicating a variable multiplicative component, almost certainly corresponding to enhanced absorption in the low state spectrum. In fact that feature can be clearly seen in the low state EPIC data in figures 6 and 7. We suggest the broad excess at ~ 1 – 2 keV can be similarly explained by greater absorption affecting the low state spectrum, lending support to our overall interpretation of the spectral change. Finally, we note that the narrow dip in the ratio plot at ~ 6.4 keV is consistent with the Fe K emission line having unchanged flux, but correspondingly higher EW in the low state spectrum.

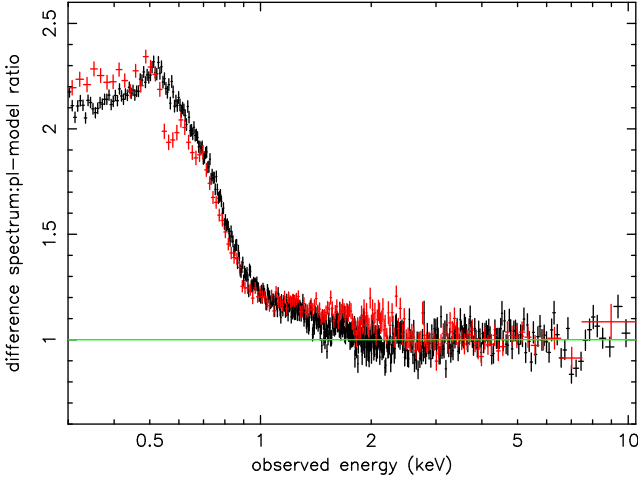


Figure 8. High minus low state difference spectral data (pn-black, M2-red) compared with a simple power law, as described in Section 5.

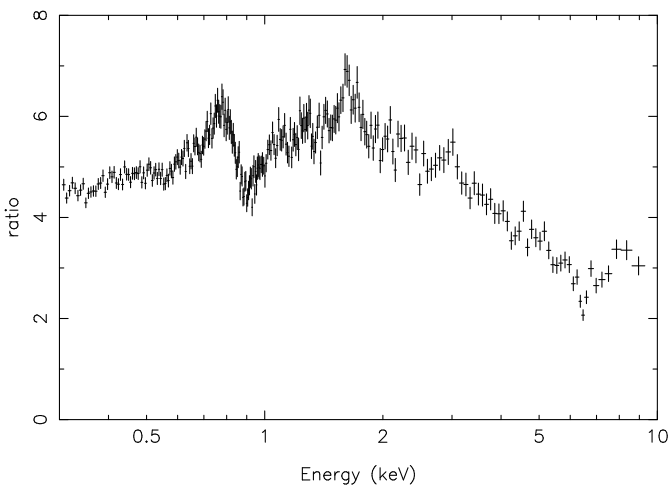


Figure 9. Ratio of high state to low state spectral data (pn only), as described in Section 5.

6 SPECTRAL LINES IN THE RGS DATA

Both EPIC spectra show a strong soft excess, with the low state (2002) spectrum also having more evidence of fine structure. To study the soft X-ray spectra in more detail we then examined the simultaneous *XMM-Newton* grating data for both observations of NGC 4051. Figures 10 and 11 reproduce the fluxed spectra, binned at 35 \AA , to show both broad and narrow features. The continuum flux level is higher in the 2001 data (consistent with the levels seen in the EPIC data), with a more pronounced curvature longwards of $\sim 15\text{ \AA}$. Numerous sharp data drops hint at the presence of many narrow absorption lines. In contrast, the 2002 November RGS spectrum exhibits a lower and flatter continuum flux, and a predominance of narrow *emission* lines.

We began an analysis of each observation by simultaneously fitting the RGS-1 and RGS-2 data with a power law and black body continuum (from the corresponding EPIC 0.3–10 keV fits) and examining the data: model residuals by eye. For the 2001 May observation the strongest features were indeed narrow absorption lines, most being readily

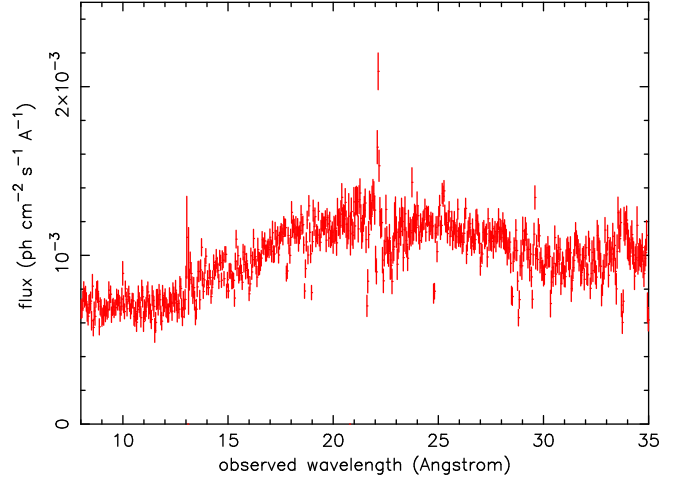


Figure 10. Fluxed RGS spectrum from the *XMM-Newton* observation of NGC 4051 in 2001 May.

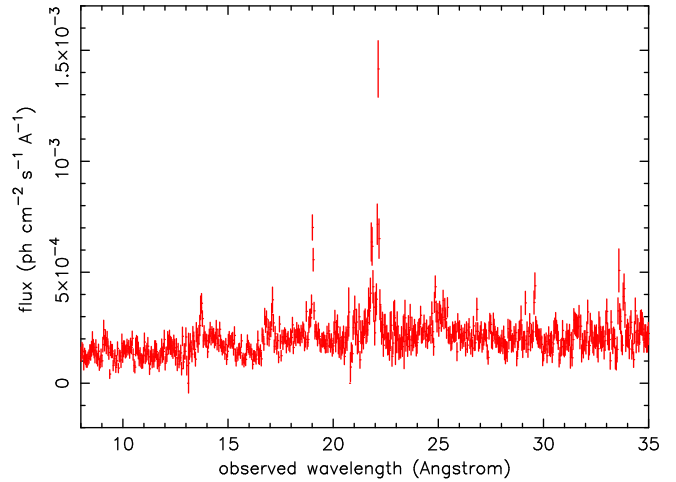


Figure 11. Fluxed RGS spectrum from the *XMM-Newton* observation of NGC 4051 in 2002 November.

identified with resonance absorption in He- and H-like ions of C, N, O and Ne. In contrast, the combined RGS data for the low state data from 2002 November showed a mainly emission line spectrum, more characteristic of a Seyfert 2 galaxy (eg Kinkhabwala et al. 2002). Significantly, the NVI, OVII and NeIX forbidden lines are seen in both high and low state RGS spectra at similar flux levels. Taking note of that fact we then analysed the low state (2002) data first, and subsequently modelled the RGS high-minus-low difference spectrum, to get a truer measure of the absorption line strengths in the high state (2001) spectrum.

6.1 An emission line spectrum in the low state data

To quantify the emission lines in the 2002 spectrum we added gaussian lines to the power law plus blackbody continuum fit in Xspec, with wavelength and flux as free parameters. In each case the line width was unresolved, indicating a $\text{FWHM} \leq 300 \text{ km s}^{-1}$. Details of the 8 strongest lines thereby identified are listed in Table 1. The statistical quality of the

fit was greatly improved by the addition of the listed lines, with a reduction in χ^2 of 251 for 16 fewer dof. When adjusted for the known redshift of NGC 4051 all the identified lines are consistent with the laboratory wavelengths indicating that the emitting gas has a mean outflow (or inflow) velocity of $\leq 200 \text{ km s}^{-1}$.

Figure 12 illustrates the OVII triplet, showing the dominant forbidden line and strong intercombination line emission, but no residual resonance line emission (at 21.6 Å). The line ratios, consistent with those found in the earlier *Chandra* observation (Collinge et al. 2001), give a clear signature of a photoionised plasma, with an electron density $\leq 10^{10} \text{ cm}^{-3}$ (Porquet and Dubau 2000). A similarly dominant forbidden line in the NVI triplet yields a density limit a factor ~ 10 lower. We note the absence of the OVII resonance emission line may be due to infilling by a residual absorption line of similar strength.

After removal of the emission lines listed in Table 1, several additional emission features (see figure 11) remained. Although narrow and barely resolved, the wavelength of these features allows them to be unambiguously identified with the radiative recombination continua (RRC) from the same He- and H-like ions of C, N, O and (probably) Ne. Table 2 lists the properties of these RRC as determined by fitting in Xspec with the REDGE model. While the RRC of CV, CVI, NVI and OVII are well determined, we fixed the other threshold energies at their laboratory values to quantify the measured equivalent widths. What is clear is that the RRC are very narrow, a combined fit yielding a mean temperature for the emitting gas of $kT \sim 3 \text{ eV}$ ($T \sim 4 \times 10^4 \text{ K}$). We note this low temperature lies in a region of thermal stability for such a photoionised gas (Krolik et al. 1981). Furthermore, the low temperature indicates collisional ionisation and excitation will be negligible, and radiative recombination should be the dominant emission process.

Additional constraints on the emitting gas in NGC 4051 can be derived by noting that the 2002 November *XMM-Newton* observation took place some 20 days after the source entered an extended low flux state. Furthermore, the emission line strength of the OVII forbidden line is essentially the same as when NGC 4051 was much brighter in 2001 May. This implies that the emission spectrum arises from ionised matter which is widely dispersed and/or of such low density that the recombination time is $\gtrsim 2 \times 10^6 \text{ s}$. At a gas temperature of $\sim 4 \times 10^4 \text{ K}$, the recombination time for OVII is of order $150(n_9)^{-1} \text{ s}$, where n_9 is the number density of the ionised matter in units of 10^9 cm^{-3} (Shull and Van Steenberg 1982). The persistent low state emission would therefore indicate a plasma density $\leq 10^5 \text{ cm}^{-3}$.

Assuming a solar abundance of oxygen, with 30 percent in OVII, 50 percent of recombinations from OVIII direct to the ground state, and a recombination rate at $kT \sim 3 \text{ eV}$ of $10^{-11} \text{ cm}^3 \text{ s}^{-1}$ (Verner and Ferland 1996), we deduce an emission measure for the forbidden line flux of order $2 \times 10^{63} \text{ cm}^{-3}$. That corresponds to a radial extent of $\gtrsim 3 \times 10^{17} \text{ cm}$ for a uniform spherical distribution of photoionised gas at the above density of $\leq 10^5 \text{ cm}^{-3}$. Coincidentally, the alternative explanation for a constant emission line flux, via an extended light travel time, also requires an emitting region scale size of $\gtrsim 10^{17} \text{ cm}$. We note, furthermore, that these values of particle density and radial distance from the ionising continuum source are consistent with the ion-

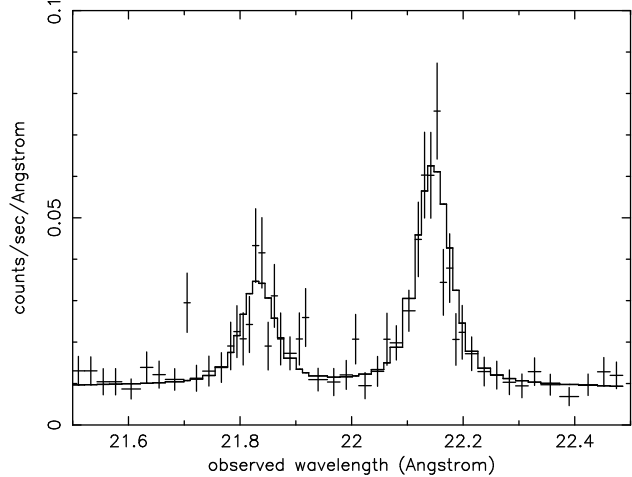


Figure 12. Emission lines dominate the 2002 November RGS data. The OVII triplet is illustrated with only the forbidden and intercombination lines clearly visible. The gaussian line fits include only the RGS resolution showing the emission lines are intrinsically narrow. See Section 6.1 for details.

sation parameter derived from our XSTAR fit to the RGS absorption spectrum (Section 7). The scale of the soft X-ray emitting gas is apparently much greater than the BLR, for which Shemmer et al. 2003 find a value of 3.0 ± 1.5 light days ($\sim 3 - 10 \times 10^{15} \text{ cm}$). In fact it has overall properties, of density, temperature and velocity consistent with the NLR in NGC 4051.

The above emission lines and RRC provide an acceptable fit to the RGS data for the 2002 November observation of NGC 4051. However a coarse binning of the data: model residuals (figure 13) shows a broad deficit of flux remaining at $\sim 15 - 17 \text{ \AA}$. It seems likely that this feature is the same as that seen in the broad band fits to the EPIC data for 2002 November (Section 4) and tentatively identified with an unresolved transition array (UTA) from Fe M-shell ions (Behar et al. 2001). When fitted with a gaussian absorption line we find an rms width of $\sigma = \sim 30 \text{ eV}$ and EW of 25 eV against the low state continuum, consistent with the absorption trough required in the partial covering fit to the low state EPIC data (section 4.2).

6.2 Absorption lines in the high state difference spectrum.

The observed wavelengths of the main emission lines in the 2002 spectrum and their equivalent absorption lines in the 2001 spectrum are the same within the resolution of our gaussian line fitting. (At higher resolution the absorption lines appear to have a mean outflow velocity of $\sim 500 \text{ km s}^{-1}$, while the emission lines are close to the systemic velocity of NGC 4051.) Furthermore, from our analysis in Section 6.1 it seems clear that the emission line spectrum represents an underlying component that responds to some long-term average flux level of the ionising continuum of NGC 4051. We therefore first subtracted the 2002 RGS spectrum from the 2001 spectrum with the aim of obtaining a truer measure of the absorption line strengths in the high state data. Quantifying the main absorption lines by adding gaussian

Table 1. Principal emission lines identified in the 2002 November RGS spectrum of NGC 4051. Wavelengths are in Angstroms and adjusted to the source rest frame and line fluxes are in units of 10^{-5} photons $\text{cm}^{-2} \text{ s}^{-1}$.

Line	λ_{source}	λ_{lab}	flux	EW (eV)
CVI Ly α	33.75 ± 0.03	33.74	4 ± 1	2.5 ± 0.6
NVI 1s-2p (f)	29.55 ± 0.04	29.53	3.5 ± 0.5	3.2 ± 0.5
NVII Ly α	24.79 ± 0.03	24.78	3 ± 0.8	3.5 ± 1
OVII 1s-2p (f)	22.14 ± 0.02	22.10	11 ± 1.5	14 ± 2
OVII 1s-2p (i)	21.79 ± 0.03	21.80	5 ± 1	6 ± 2
OVIII Ly α	18.99 ± 0.03	18.97	8 ± 1.3	10 ± 1.5
FeXVII 2p-3s	17.06 ± 0.03	17.2	2 ± 0.6	5 ± 2
NeIX 1s-2p (f)	13.75 ± 0.05	13.70	3 ± 0.6	7 ± 2

Table 2. Radiative recombination continua identified in the 2002 November RGS spectrum of NGC 4051. All wavelengths are in Angstroms and line fluxes are in units of 10^{-5} photons $\text{cm}^{-2} \text{ s}^{-1}$. The threshold wavelengths fixed (f) at the laboratory values are as indicated.

RRC	λ_{source}	λ_{lab}	flux	EW (eV)
NeX	9.13 (f)	9.11	0.3 ± 0.2	6 ± 4
NeIX	10.39 (f)	10.37	0.75 ± 0.3	13 ± 5
OVIII	14.19 (f)	14.15	1.7 ± 0.5	9 ± 3
OVII	16.85	16.81	3.2 ± 0.8	11 ± 3
NVI	22.50	22.45	1.7 ± 0.8	2 ± 1
CVI	25.41	25.35	5.7 ± 1	7 ± 1
CV	31.71	31.64	2 ± 1.5	3 ± 2

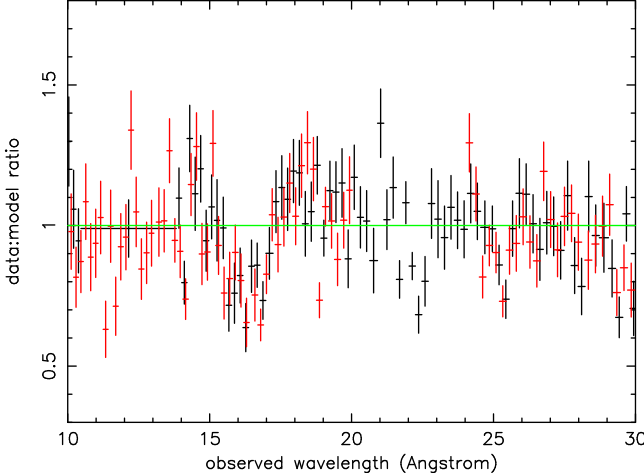


Figure 13. Ratio of the 2002 November RGS data to the emission line and RRC model described in Section 6.1. A broad deficit of flux at $\sim 15 - 17 \text{ \AA}$ may be attributed to an unresolved transition array (UTA) in weakly ionised Fe.

lines to the corresponding continuum fit then produced the line list in Table 3.

7 AN IONISED ABSORBER MODEL FIT TO THE 2001 MAY *XMM-Newton* DATA.

To better quantify the highly ionised matter responsible for the observed absorption features in the ‘high flux state’ spectrum of NGC 4051 and check for physical consistency of the candidate line identifications, including the high energy absorption features seen above 7 keV in the EPIC data, we next

replaced the gaussian absorption lines in the above fits with a model comprising a grid of photoionised absorbers based on the XSTAR code (Kallman et al. 1996). We modelled the RGS difference spectrum as the best measure of low ionisation matter; however, in the case of the EPIC data, where we expect the particle density to be higher (and recombination time shorter) than in the extended emission region, we modelled the direct high state data. The XSTAR model absorbers cover a wide range of column density and ionisation parameter, with outflow (or inflow) velocities as a variable parameter. All abundant elements from C to Fe are included with the relative abundances as a variable input parameter. To limit processing time we assumed a fixed width for each absorption line of 1000 km s^{-1} FWHM.

We first attempted a fit to the RGS data over the $8.5 - 35 \text{ \AA}$ band, where the power law plus blackbody continuum gave χ^2 of 5388 for 4197 dof. The addition of a two-component ionised absorber significantly improved this fit, to χ^2 of 4829/4183, with an ionisation parameter $\log \xi$ of 2.7 ± 0.1 and column density of $N_H \sim 6 \times 10^{21} \text{ cm}^{-2}$, and an ionisation parameter $\log \xi$ of 1.4 ± 0.1 and column density of $N_H \sim 2 \times 10^{21} \text{ cm}^{-2}$. The relative abundances of C,N,O,Ne, and Fe, tied for both components, were determined to be 0.5, 0.6, 0.35, 0.3 and 1.0. The apparent redshift from the fit was $5.2 \pm 1.4 \times 10^{-4}$, indicating an outflow velocity of $\sim 600 \text{ km s}^{-1}$ at the redshift of NGC 4051. We note this velocity is probably a lower limit for those lines where a significant emission component has been subtracted. While the present analysis is only intended to obtain a rough characterisation of the low ionisation outflow, several points stand out.

A significantly better fit with the 2-component absorber suggests a range of ionisation parameter exists in the outflow, a point emphasised more strongly when the Fe-K absorption line is added (see below). As noted earlier the

Table 3. Principal absorption lines identified in the 2001 May RGS ‘difference’ spectrum of NGC 4051. The Ne IX resonance line appears to be broad and is probably blended with Fe XIX. Wavelengths are in Angstroms and adjusted to the source restframe

Line	λ_{source}	λ_{lab}	EW (mA)
CVI Ly α	33.67 \pm 0.02	33.74	170 \pm 30
CVI Ly β	28.42 \pm 0.02	28.47	60 \pm 15
CVI Ly γ	26.95 \pm 0.03	26.99	20 \pm 10
NVI 1s-2p	28.73 \pm 0.02	28.79	80 \pm 15
NVII Ly α	24.73 \pm 0.03	24.79	100 \pm 25
OVIII Ly α	18.93 \pm 0.01	18.97	100 \pm 15
OVIII Ly β	15.98 \pm 0.02	16.01	25 \pm 10
OVII 1s-2p	21.57 \pm 0.03	21.60	60 \pm 15
OVII 1s-3p	18.62 \pm 0.03	18.63	40 \pm 112
OVII 1s-4p	17.76 \pm 0.04	17.77	15 \pm 8
NeIX 1s-2p	13.43 \pm 0.03	13.45	40 \pm 15

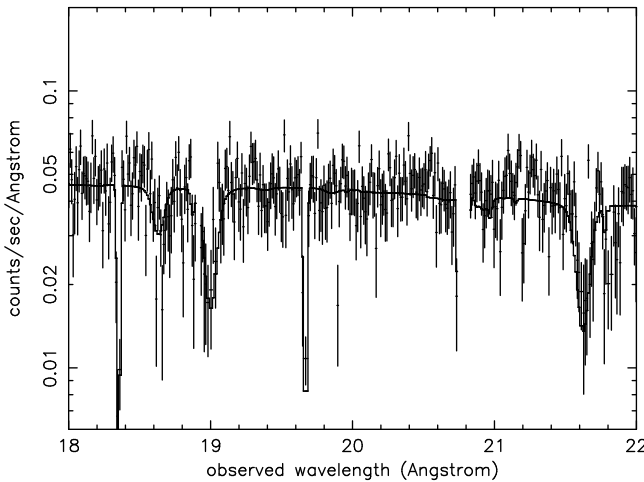


Figure 14. Part of the 2001 May RGS ‘difference’ spectrum fitted with the photoionised absorber model described in Section 7. The main absorption lines shown are, from the right, OVII 1s-2p (21.60Å), OVIII Ly α (18.97Å) and OVII 1s-3p (18.63Å)

strongest observed lines are all from H- and He-like ions of the lighter metals. The model is seen to fit the the resonance lines of OVII and OVIII quite well (figure 14), perhaps since these strongest lines drive the fit. However, the higher series lines of OVII are noticeably stronger than in the model, suggesting the resonance line is saturated in the core.

The \sim 7.1 keV absorption line, most conservatively attributed to blue-shifted FeXXVI Ly α resonance absorption, required a third, more highly ionised component in the absorbing gas, with ionisation parameter $\log\xi\sim 3.8$ and column density of $N_H\sim 2\times 10^{23}\text{cm}^{-2}$. The apparent redshift from the fit was -0.02, indicating an outflow velocity of $\sim 6500 \text{ km s}^{-1}$ at the redshift of NGC 4051. The ionisation parameter, and hence column density, are not well constrained by this single line fit. However, the main uncertainty in the column probably lies on the upside, since the line is apparently broader than in the XSTAR model fit, while the fitted ionisation parameter is close to that for a peak abundance of FeXXVI. Assuming a cone angle for the highly ionised outflow of $\pi \text{ sr}$, the corresponding outflow mass rate is $\sim 7\times 10^{-3} \text{ M}_\odot \text{yr}^{-1}$, with an associated kinetic energy of $\sim 10^{41} \text{ erg s}^{-1}$, comparable to the high (mean) state hard X-ray luminosity of NGC 4051.

Repeating the XSTAR fit for the only likely alternative identification of the \sim 7.1 keV line, with the resonance (1s-2p) absorption of Fe XXV, required a lower ionisation parameter for the third component, of $\log\xi=3.3\pm 0.1$ together with a column density of $N_H\sim 10^{23}\text{cm}^{-2}$. The apparent redshift from the fit was -0.058, indicating an outflow velocity of $\sim 16500 \text{ km s}^{-1}$ at the redshift of NGC 4051. Again assuming a cone angle of the highly ionised outflow of $\pi \text{ sr}$, the corresponding outflow mass rate is then $\sim 5\times 10^{-2} \text{ M}_\odot \text{yr}^{-1}$, with a kinetic energy of $2\times 10^{42} \text{ erg s}^{-1}$.

8 AN IONISED ABSORBER MODEL FIT TO THE 2002 NOVEMBER EPIC DATA.

Implicit in our analysis so far is the constant nature of the extended, low ionisation gas. In contrast, our partial covering fit to the low state EPIC data requires a substantial column density in a lower ionisation state (than in the high state EPIC fit), covering \sim 60 per cent of the hard X-ray continuum source. It seems a reasonable assumption that this new absorbing component is formed from the previously highly ionised outflow as the ionisation parameter falls with the reduced hard X-ray flux. To quantify this change, and obtain an alternative fit to the overall low state spectrum of NGC 4051, we then replaced the ABSORI model of section 5 with XSTAR.

The result supports the ABSORI fitting. Figure 15 illustrates the XSTAR fit to the low state EPIC data, the parameters being, a power law of $\Gamma= 1.93\pm 0.03$, \sim 57 per cent of which is covered by a column of $N_H\sim 3.6\times 10^{23}\text{cm}^{-2}$ and intermediate ionisation parameter $\log\xi=1.4\pm 0.1$. The remaining power law component, a black body of $kT \sim 125 \text{ eV}$, and a narrow Fe K emission line are covered by an ionised absorber similar to that fitted to the RGS high state data, with $\log\xi\sim 2.8$ and $N_H\sim 8\times 10^{21}\text{cm}^{-2}$, together with a cold column of $\sim 2\times 10^{20} \text{ cm}^{-2}$, slightly greater than the Galactic column. It is interesting to note that a similar high column density is required for EPIC fits in both high and low states, with the dramatic spectral change being attributed to part of that matter recombining in response to the lower hard X-ray flux. Furthermore, when left as a free parameter, the power law slope in the partial covering fit has a preferred value consistent with that in the high state. In other words, the second important initial assumption we made in section

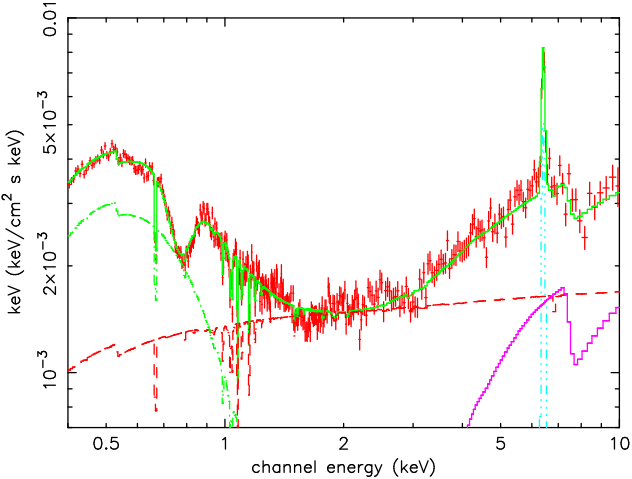


Figure 15. The XSTAR 0.3–10 keV partial covering fit to the low state 2002 November observation of NGC 4051, showing the strong soft excess and a broad absorption trough at ~ 0.76 keV. Also shown are the separate components in the fit: the unabsorbed power law (red), absorbed power law (pink), Gaussian emission line (blue) and blackbody (green). For clarity only the pn data are shown.

5 (in addition to constant cold reflection) is also supported in this analysis.

9 DISCUSSION

9.1 Hard X-ray emission and re-processing in outflowing gas.

Given the general acceptance that AGN are powered by accretion onto a supermassive black hole it seems reasonable that the usually-dominant optical-XUV flux arises as thermal radiation from the accretion disc. However, the origin of the hard X-ray power law component (and soft X-ray excess) remains less clear, with up-scattering of disc photons in a high temperature ‘corona’ being a popular mechanism. The strengthening view that viscosity in the disc is largely of magnetic origin offers an appealing way of transferring accretion energy to the coronal electrons by re-connection in buoyant magnetic flux. Reprocessing of hard X-rays in the disc may then explain a major part of the ‘continuum reflection’ and fluorescent Fe K emission often seen in AGN spectra.

The most direct evidence given in support of this picture has usually been the rapid, high amplitude X-ray variability (implying a small emission region) and the broad, skewed profile of the Fe K line, indicating an origin in reflection from the innermost accretion disc where strong relativistic effects are expected. Recently some doubts have been raised on the wide applicability of this model. In particular, improved X-ray spectra from *Chandra* and *XMM-Newton* have failed to confirm the relativistic Fe K emission line in a majority of AGN. Furthermore, new evidence of massive outflows of highly ionised matter in a number of AGN has drawn attention to the need to take due account of re-processing in overlying (as well as disc) matter. While in the previous cases where high velocity outflows have been confirmed they appear to be linked to a high (Eddington

or super-Eddington) accretion rate, the evidence for column densities of highly ionised gas in excess of $N_H \sim 10^{23} \text{ cm}^{-2}$ is becoming more common for Seyfert 1 galaxies (eg Bianchi et al. 2003). Such columns then potentially offer an alternative explanation to the extreme broad Fe K line, via partial covering of the power law continuum. In the present analysis of the *XMM-Newton* observations of NGC 4051 we have explored the partial covering alternative, noting that the observation of FeXXVI (or Fe XXV) absorption in the high state requires a similar column density (of highly ionised gas), which would have recombined as a result of the reduced ionising flux persisting for ~ 20 days prior to the 2002 November observation. We conclude that variable opacity in this outflow, responding to the reduced ionising flux during the extended low state of NGC 4051, provides a natural explanation of the dramatic change observed in the broad band X-ray spectrum of NGC 4051. We suggest that the effects of absorption by line-of-sight ionised gas may have been generally underestimated in the analysis and interpretation of AGN spectra, and note that a similar explanation was proposed by Costantini et al. (2001) in reporting a large scale spectral change in the Seyfert galaxy NGC3516 observed in two *BepoSAX* observations 4 months apart.

The important detection of a high velocity outflow in the high state spectrum of NGC 4051 (given independent support by the recent report of an outflow at 4500 km s^{-1} from a second *Chandra* observation; van der Meer et al. 2003) raises the additional question of what fraction of the hard X-ray emission may arise, not from the disc/corona, but from shocks in this flow? We showed in Section 7 that if the inner flow has a wide cone angle, the associated kinetic energy is comparable with the hard X-ray luminosity in NGC 4051. If the trigger for a massive outflow is - as suggested by King and Pounds (2003a) - accretion at or above the Eddington limit, then might this apply for NGC 4051? A recent reverberation measurement (Shemmer et al. 2003) has indicated the black hole mass in NGC 4051 to lie between $2 - 10 \times 10^5 \text{ M}_\odot$, an unusually low value (for an AGN), but one supported by a further recent analysis of the X-ray variability (McHardy et al. 2003). Such a low mass suggests that in the ‘typical’ bright state of NGC 4051, as we observed in 2001 May when the total X-ray luminosity was $\sim 10^{42} \text{ erg s}^{-1}$, the bolometric luminosity of NGC 4051 might indeed have reached, or exceeded, the Eddington limit.

9.2 Extended photoionised gas in NGC 4051.

The low central continuum flux during the 2002 November observation of NGC 4051 allowed the emission spectrum from an extended photoionised gas to be observed in the RGS data, a rare opportunity to observe this component in a Seyfert 1 galaxy (see also Turner et al. 2003 for a similar observation of NGC 3516). The detection of several RRC show the temperature of the gas to be $\leq 5 \times 10^4 \text{ K}$, a region of thermal stability, while our analysis of the strong forbidden line emission of OVII provides an estimate of the (minimum) extent as $3 \times 10^{17} \text{ cm}$. A corresponding minimum mass for this extended gas envelope is then $\sim 10 \text{ M}_\odot$. Assuming a mean outflow velocity of 100 km s^{-1} , the flow time (to reach $3 \times 10^{17} \text{ cm}$) is $\sim 10^3$ years. It is interesting to note that the mass of the extended low ionisation region would be re-

plenished in a similar timescale if fed by the higher velocity outflow (observed as FeXXVI Ly α absorption at ~ 7.1 keV).

9.3 A common outflow

Continuing this line of thought we consider how the various components of the overlying gas indicated by the X-ray spectra of NGC 4051 may be parts of the same common outflow. On the (simplest) assumption of a quasi-spherical outflow and conservation of mass, we envisage the high velocity/high ionisation flow (imprinting absorption features in the Fe K band), degrading into the intermediate ionisation/lower velocity flow (seen in the RGS absorption lines), before eventually connecting with the larger scale/slow moving outflow observed in emission in the low state RGS data. It is interesting to then speculate that this slowly recombining, low density gas will link into the larger scale outflow resolved in the [OIII]5007 Å line and co-spatial with weak extended radio emission (Christopoulou et al. 1997).

We assume the FeXXVI Ly α interpretation of the 7.1 keV absorption line, at an outflow velocity v of $\sim 6 \times 10^8$ cm s $^{-1}$. With an ionising luminosity $\sim 2 \times 10^{41}$ erg s $^{-1}$ and $\log \xi = 3.8$, the product nr^2v is then $\sim 2 \times 10^{46}$ cm $^{-3}$ s $^{-1}$. Conservation of mass in a radial flow maintains this value to eventually connect with the intermediate and low ionisation components fitted to the RGS high state spectra. Assuming each absorbing layer is of thickness $0.3r$, the measured column density also allows the mean particle density (n) and radial distance (r) from the ionising source to be evaluated, yielding $n \sim 1.2 \times 10^{10}$ cm $^{-3}$ and $r \sim 5 \times 10^{13}$ cm for the highly ionised flow.

For the intermediate ionisation gas, responsible for most of the observed RGS absorption lines, the measured ionisation parameter and column density (together with $nr^2v = 2 \times 10^{46}$ cm $^{-3}$ s $^{-1}$) yield $v \sim 5 \times 10^7$ cm s $^{-1}$, consistent with the value obtained from the mean line ‘blueshift’, together with $n \sim 10^6$ cm $^{-3}$ and $r \sim 3 \times 10^{16}$ cm.

For the lower ionisation component in our XSTAR fit to the RGS absorption lines, the same procedure yields $v \sim 2.5 \times 10^6$ cm s $^{-1}$, essentially the systemic velocity indicated by the emission line spectrum, together with $n \sim 3 \times 10^3$ cm $^{-3}$ and $r \sim 3 \times 10^{18}$ cm, again approximately in agreement with the scale deduced independently from the emission line spectrum.

On this continuous outflow picture the kinetic energy in the initial outflow is largely lost before reaching the intermediate ionisation stage, and we speculate that this could be due to shocks occurring in the high velocity gas, potentially contributing a significant part of the hard X-ray luminosity. We note that the derived particle densities will ensure a rapid response to changing flux in the inner regions of the flow, while the intermediate ionisation gas indicated by the RGS data will already have a recombination time $\gtrsim 4$ days.

Important questions that remain from this exploration of the complex X-ray spectrum of NGC 4051 include, the mechanism by which the high velocity outflow is generated and the origin of the soft X-ray excess. These questions will be addressed in a separate paper (King and Pounds 2003b).

9.4 Absorption or spectral pivoting

Since this paper was initially submitted, an independent analysis of the 2002 November low state data (pn camera only) has been accepted for publication in MNRAS (Uttley et al. 2003). That analysis is guided by the flux-flux plots which, unusually in the case of NGC 4051, suggest spectral variability is primarily due to pivoting of the power law spectrum. On that basis Uttley et al. develop a model for the low state pn spectrum which contains both variable and constant thermal components to describe the ‘soft excess’. Their model also includes a ‘constant’ reflection components and ionised absorption, as does our spectral fit. However, the major difference in the two approaches is that Uttley et al. explain the main spectral change by a large change in the power law slope, whereas in the present paper we emphasise the dominant effects of variable absorption in a substantial column of line-of-sight photoionised gas.

Our analysis has the advantage of including simultaneous high resolution data from the RGS, revealing the presence of an extended outflow of photoionised gas which we show to be a reasonable continuation of a high density flow at small radii. More direct evidence for a large column density of ionised gas in line of sight to the X-ray source comes from the detection of a blue-shifted FeXXVI Ly α absorption line in high state EPIC data (also not considered in Uttley et al. 2003). We suggest it is then a natural outcome for that gas to have recombined during the period of low X-ray emission to give the enhanced absorption implied in our fit to the low state spectrum of NGC 4051.

10 SUMMARY

(1) During a typical bright state the X-ray spectrum of the low mass AGN NGC 4051 is found to be characteristic of a Seyfert 1 galaxy, with a canonical power law slope $\Gamma \sim 1.9$ plus cold reflection (and narrow Fe K emission line), together with a soft excess superimposed on which is an absorption line spectrum consistent with an outflow of ~ 500 km s $^{-1}$. An additional spectral feature, not hitherto reported, is a deep absorption line at ~ 7.1 keV, indicating a higher velocity, more highly ionised and higher column density outflow component.

(2) A second *XMM-Newton* observation of NGC 4051, 20 days into a period of unusually faint X-ray emission, exhibits a very different spectrum. In the soft X-ray band the absorption line spectrum is replaced with an emission line spectrum more characteristic of a Seyfert 2, which we model as an extended, low density region of photoionised gas. At higher energies the indicators of cold reflection (including the narrow Fe K emission line) are unchanged, but the continuum exhibits strong curvature which we interpret in terms of partial covering by a substantial column density of intermediate ionisation.

(3) We conclude that the unusually hard X-ray spectrum of NGC 4051 in 2002 November is due to the enhanced visibility of a ‘constant’ cold reflection component and increased opacity in a substantial column of line-of-sight gas responding to an extended period of low hard X-ray emission.

ACKNOWLEDGEMENTS

The results reported here are based on observations obtained with *XMM-Newton*, an ESA science mission with instruments and contributions directly funded by ESA Member States and the USA (NASA). The authors wish to thank Paul O'Brien, Martin Elvis and Simon Vaughan for valuable input, the SOC and SSC teams for organising the *XMM-Newton* observations and initial data reduction, and the referee for a careful and constructive reading of the text. KAP acknowledges the support of a Leverhulme Trust Emeritus Fellowship.

REFERENCES

Arnaud K.A. 1996, ASP Conf. Series, 101, 17

Behar E., Sako M., Kahn S.M. 2001, ApJ, 563, 497

Bianchi S., Matt G., Balestra I., Perola G.C. 2003, A&A, 407, L21

Chartas G., Brandt W.N., Gallagher S.C., Garmire G.P. 2002, ApJ, 569, 179

Christopoulou P.E., Holloway A.J., Steffen W., Mundell C.G., Thean A.H.C., Goudis C.D., Meaburn J., Pedlar A. 1997, MNRAS, 284, 385

Collinge M.J. et al. 2001, ApJ, 557, 2

Costanini E. et al. 2001, ApJ, 544, 283

den Herder J.W. et al. 2001, A&A, 365, L7

Elvis M., Lockman F.J., Wilkes B.J. 1989, AJ, 97, 777

Fabian A.C., Vaughan S. 2003, MNRAS 340, L28

Guainazzi M., Mihara T., Otani C., Matsuoka M. 1996, PASJ, 48, 781

Guainazzi M. et al. 1998, MNRAS, 301, L1

Kallman T., Liedahl D., Osterheld A., Goldstein W., Kahn S. 1996, ApJ, 465, 994

Kaspi S. et al. 2002, ApJ, 574, 643

King A.R., Pounds K.A. 2003a, MNRAS, 345, 657

King A.R., Pounds K.A. 2003b, MNRAS, in preparation

Kinkhabwala A. et al. 2002, ApJ, 575, 732

Komossa S., Fink H. 1997, A&A, 322, 719

Krolik J., McKee C.F., Tarter J. 1981, ApJ, 249, 422

Kunieda H., Hayakawa S., Tawara Y., Koyama K., Tsuruta S., Leighly K. 1992, ApJ, 384, 482

Lamer G., McHardy I.M., Uttley P., Jahoda K. 2003, MNRAS, 338, 323

Lawrence A., Pounds K.A., Watson M.G., Elvis M. 1985, MNRAS, 217, 685

Lawrence A., Watson M.G., Pounds K.A., Elvis M. 1987, Nature, 325, 694

McHardy I.M., Green A.R., Done C., Puchnarewicz E.M., Mason K.O., Branduardi-Raymont G., Jones M.H. 1995, MNRAS, 273, 549

McHardy I.M., Papadakis I.E., Uttley P., Mason K.O., Page M.J. 2003, astro-ph/0309180

Magdziarz P., Zdziarski A.A. 1995, MNRAS, 273, 837

Matsuoka M., Piro L., Yamauchi L., Murakami T. 1990, ApJ, 361, 440

Nandra K., Pounds K.A., Stewart G.C., Fabian A.C., Rees M.J. 1989, MNRAS, 236, 39

Nandra K., Pounds K.A. 1994, MNRAS, 268, 405

Porquet D., Dubau J. 2000, A&A, 343, 495

Pounds K.A., Nandra K., Stewart G.C., George I.M., Fabian A.C. 1990, Nature, 344, 132

Pounds K.A., Nandra K., Fink H.H., Makino F. 1994, MNRAS, 267, 193

Pounds K.A., Reeves J.N. 2002, in: *New Visions of the X-ray Universe in the XMM-Newton and Chandra era* ed. F. Jansen, (astro-ph/0201436)

Pounds K.A., Reeves J.N., King A.R., Page K.L., O'Brien P.T., Turner M.J.L. 2003a, MNRAS, 345, 705

Pounds K.A., King A.R., Page K.L., O'Brien P.T. 2003b, MNRAS, 346, 1025

Reeves J.N., O'Brien P., Ward M.J. 2003, ApJ, 593, L65

Sako M. et al. 2001, A&A, 365, L168

Shemmer O., Uttley P., Netzer H., McHardy I.M. 2003, MNRAS, 343, 1341

Shull J.M., Van Steenberg M. 1982, ApS, 48, 95 (erratum 49, 351)

Strüder L. et al. 2001, A&A, 365, L18

Taylor R.D., Uttley P., McHardy I.M. 2003, MNRAS, 342, L31

Turner M.J.L. et al. 2001, A&A, 365, L27

Turner T.J., Kraemer S.B., Mushotzky R.F., George I.M., Gabel J.R. 2003, ApJ, 594, 128

Uttley P., Taylor R.D., McHardy I.M., Page M.J., Mason K.O., Lamer G., Fruscione A. 2003, MNRAS - accepted (astro-ph/0309179)

van der Meer R.L.J., Kaastra J.S., Steenbrugge K.C., Komossa S. 2003, ASP Conf. Series, 290, 133

Verner D.A., Ferland G.J. 1996, ApJS, 103, 467